In vivo imaging of axonal transport of mitochondria in the diseased and aged mammalian CNS

Yuji Takihara[a,b], Masaru Inatani[a,b,1], Kei Eto[c,d], Toshihiro Inoue[b], Alexander Kreymerman[e], Seiji Miyake[a], Shinji Ueno[f], Masatoshi Nagaya[f], Ayami Nakanishi[f], Keiichiro Iwao[b], Yoshihiro Takamura[a], Hirotaka Sakamoto[g], Keita Satoh[g], Mineo Kondo[h], Tatsuya Sakamoto[g], Jeffrey L. Goldberg[e], Junichi Nabekura[c,d], and Hidenobu Tanihara[b]

[a]Department of Ophthalmology, Faculty of Medical Science, University of Fukui, Fukui 910-1193, Japan; [b]Department of Ophthalmology, Faculty of Life Sciences, Kumamoto University, Kumamoto 860-8556, Japan; [c]Division of Homeostatic Development, Department of Developmental Physiology, National Institute for Physiological Sciences, Aichi 444-8585, Japan; [d]Department of Physiological Sciences, SOKENDAI (The Graduate University for Advanced Studies), Aichi 444-8585, Japan; [e]Shiley Eye Institute, University of California, San Diego, La Jolla, CA 92093; [f]Department of Ophthalmology, Nagoya University Graduate School of Medicine, Nagoya 466-8550, Japan; [g]Ushimado Marine Institute, Graduate School of Natural Science and Technology, Okayama University, Okayama 701-4303, Japan; and [h]Department of Ophthalmology, Mie University Graduate School of Medicine, Mie 514-8507, Japan

Edited by Thomas L. Schwarz, Children's Hospital, Boston, MA, and accepted by the Editorial Board July 13, 2015 (received for review May 27, 2015)

The lack of intravital imaging of axonal transport of mitochondria in the mammalian CNS precludes characterization of the dynamics of axonal transport of mitochondria in the diseased and aged mammalian CNS. Glaucoma, the most common neurodegenerative eye disease, is characterized by axon degeneration and the death of retinal ganglion cells (RGCs) and by an age-related increase in incidence. RGC death is hypothesized to result from disturbances in axonal transport and in mitochondrial function. Here we report minimally invasive intravital multiphoton imaging of anesthetized mouse RGCs through the sclera that provides sequential time-lapse images of mitochondria transported in a single axon with submicrometer resolution. Unlike findings from explants, we show that the axonal transport of mitochondria is highly dynamic in the mammalian CNS in vivo under physiological conditions. Furthermore, in the early stage of glaucoma modeled in adult (4-mo-old) mice, the number of transported mitochondria decreases before RGC death, although transport does not shorten. However, with increasing age up to 23–25 mo, mitochondrial transport (duration, distance, and duty cycle) shortens. In axons, mitochondria-free regions increase and lengths of transported mitochondria decrease with aging, although totally organized transport patterns are preserved in old (23- to 25-mo-old) mice. Moreover, axonal transport of mitochondria is more vulnerable to glaucomatous insults in old mice than in adult mice. These mitochondrial changes with aging may underlie the age-related increase in glaucoma incidence. Our method is useful for characterizing the dynamics of axonal transport of mitochondria and may be applied to other submicrometer structures in the diseased and aged mammalian CNS in vivo.

mammalian CNS | in vivo imaging | mitochondrial axonal transport | neurodegeneration | aging

Globally, longevity is increasing, and the cohort aged 60 y or over is the fastest growing portion of the population. These trends place neurodegenerative diseases among the greatest clinical threats. Glaucoma, the most common progressive neurodegenerative eye disease (1), globally affects an estimated 60.5 million people, of whom 8.4 million are bilaterally blind (2). Similar to other neurodegenerative diseases of the CNS, including Alzheimer's disease (3) and Parkinson's disease (4), the incidence of glaucoma (5) increases with aging. Glaucoma is characterized by axon degeneration and the death of retinal ganglion cells (RGCs) (6). Histological studies in glaucoma models have suggested disturbances in the axonal transport of mitochondria in RGCs (7, 8).

Axonal transport is essential for delivering the organelles and proteins that are required for axonal function and maintenance. Mitochondria are organelles that must be transported in axons and distributed appropriately to function (9, 10), because mitochondria play a pivotal role in the function and survival of neurons by generating ATP, maintaining Ca^{2+} and reduction-oxidation (redox) homeostasis, and signaling in apoptosis. Disturbances in mitochondrial dynamics are suggested to be involved in neurodegenerative diseases and CNS aging (11–14). In vivo imaging of axonal transport of mitochondria has been reported using explant imaging of the *Drosophila* nervous system (15) and rat cerebellar slice cultures (16) and intravital imaging (direct in vivo imaging of living animals at subcellular resolution) of the mouse peripheral nervous system (17) and zebrafish nervous system (18). However, intravital imaging of axonal transport of mitochondria has not been achieved in the mammalian CNS. Importantly, the lack of intravital imaging of axonal transport of mitochondria in the mammalian CNS under physiological oxygen levels and metabolism and with intact blood flow has precluded the characterization of the dynamics of axonal transport of mitochondria in the CNS of diseased and aged mammals in vivo.

To perform intravital imaging of axonal transport of mitochondria in the mammalian CNS, we developed the technique we call "MIMIR" (for "minimally invasive intravital imaging of mitochondrial axonal transport in RGCs"). MIMIR does not involve thinning or opening of the sclera or produce changes in

Significance

The lack of intravital imaging of axonal transport of mitochondria in the living mammalian CNS precludes the characterization of transport dynamics in the diseased and aged mammalian CNS. Here we report minimally invasive intravital multiphoton imaging of mouse retinal ganglion cells that offers sequential time-lapse images of mitochondria transported in a single axon with submicrometer resolution. We show highly dynamic axonal transport of mitochondria in the mammalian CNS in vivo under physiological conditions and characterize disturbances of mitochondrial transport in a mouse glaucoma model and age-related changes in mitochondrial transport. Our method is useful for characterizing the dynamics of axonal transport of mitochondria and the dynamics of other submicrometer structures in the diseased and aged mammalian CNS in vivo.

Author contributions: Y. Takihara, M.I., and J.L.G. designed research; Y. Takihara, M.I., K.E., T.I., A.K., S.M., S.U., M.N., A.N., K.I., Y. Takamura, H.S., K.S., M.K., T.S., J.N., and H.T. performed research; Y. Takihara, M.I., K.E., and J.N. contributed new reagents/analytic tools; Y. Takihara, M.I., K.E., T.I., A.K., S.M., S.U., M.N., A.N., K.I., Y. Takamura, H.S., K.S., M.K., T.S., J.L.G., J.N., and H.T. analyzed data; and Y. Takihara and M.I. wrote the paper.

The authors declare no conflict of interest.

This article is a PNAS Direct Submission. T.L.S. is a guest editor invited by the Editorial Board.

Freely available online through the PNAS open access option.

[1]To whom correspondence should be addressed. Email: inatani@u-fukui.ac.jp.

This article contains supporting information online at www.pnas.org/lookup/suppl/doi:10.1073/pnas.1509879112/-/DCSupplemental.

the intraocular humor. MIMIR directly showed, at submicrometer resolution, that axonal transport of mitochondria is highly dynamic in the mammalian CNS in vivo under physiological conditions. It enabled us to characterize disturbances of mitochondrial transport in a mouse model of glaucoma and age-related changes of mitochondrial transport in old (23- to 25-mo-old) mice.

Results

Axonal Transport of Mitochondria Can Be Detected by Explant Imaging of the Mouse Retina. To detect axonal transport of mitochondria in the mammalian CNS in vivo, we chose RGCs that extend their axons into the nerve fiber layer. We hypothesized that RGCs would be advantageous for detecting the axonal transport of mitochondria in vivo because the sheet structure of the nerve fiber layer is parallel to the ocular surface of the sclera (*SI Appendix*, Fig. S1*A*, blue). Acquiring four-dimensional sequential time-lapse images of mitochondria transported in a single axon in vivo is not required, because it is possible to keep the plane of the nerve fiber layer parallel to the *x,y*-plane of intravital imaging. First, we sought conditions in which RGCs expressed fluorescent proteins in mitochondria sparsely enough to identify individual RGC axons, because the ubiquitous distribution of mitochondria in the CNS prevents following continuous mitochondrial transport in a single axon in vivo. Using immunohistochemistry, we found that the sparse expression of CFP in RGCs of *Thy1-mitoCFP-S* mice (17) allowed us to identify a single RGC axon (*SI Appendix*, Fig. S1 *B* and *C*) that projected to the optic nerve head (ONH). Immunogold labeling of the nerve fiber layer indicated that CFP was expressed specifically in mitochondria in part of the RGC axons in *Thy1-mitoCFP-S* mice (*SI Appendix*, Fig. S1 *D* and *E*). Interestingly, explant multiphoton imaging of the retina of *Thy1-mitoCFP-S* mice detected transport of mitochondria in an RGC axon (*SI Appendix*, Fig. S2 and Movie S1).

Intravital Imaging of the Mouse Retina Through the Sclera Shows Individual RGC Axons. Next, we investigated whether a single RGC axon could be identified by intravital imaging of the mouse retina. Functional adaptive optics cellular imaging in the living eye shows the mouse RGC soma and neurites in vivo (19). We found that minimally invasive opening of the skin (asterisk in *SI Appendix*, Fig. S3*A*) and conjunctiva (the area surrounded by arrows in *SI Appendix*, Fig. S3*A*), without opening the sclera, in an albino line of *Thy1-mitoCFP-S* mice considerably improves the accessibility (i.e., minimal absorption and scattering of light) of the mouse retina, making the accessibility of the mouse retina similar to that of the zebrafish CNS for intravital imaging (*SI Appendix*, Fig. S3*A*). Taking advantage of this excellent accessibility, we developed minimally invasive intravital imaging of the mouse retina through the sclera (*SI Appendix*, Fig. S3*B*). *Z*-stack images of minimally invasive intravital imaging of the mouse retina through the sclera (the area surrounded by arrows in *SI Appendix*, Fig. S3*A*) obtained using a multiphoton microscope showed distinct layers in the retina, including the retinal pigment epithelium, deeper layer of the retinal vascular system, inner nuclear layer, inner plexiform layer, RGC cell bodies and dendrites in the ganglion cell layer, and RGC axons in the nerve fiber layer (*SI Appendix*, Fig. S3 *C*–*H* and Movie S2). Individual RGC axons commonly projected to the ONH (*SI Appendix*, Fig. S3*H*). 3D images (*SI Appendix*, Fig. S3*I* and Movie S3) from the inner plexiform layer to the nerve fiber layer show the entire RGC (arrowhead in *SI Appendix*, Fig. S3*G*), including the RGC axon and dendrites, at subcellular resolution.

Highly Dynamic Axonal Transport of Mitochondria in the Mammalian CNS in Vivo Under Physiological Conditions. For intravital imaging of axonal transport of mitochondria, the following conditions are necessary: sequential time-lapse images of mitochondria transported in a single axon with submicrometer resolution; focus on the axon maintained without artifacts caused by heartbeat and breathing; a short time-lapse interval; and avoidance of phototoxicity. The diameters of the axonal shafts between varicosities in rodents range from 0.1–0.3 μm (20). A seminal study of mice showed the storage structures of the retinal pigment epithelium in vivo without opening the sclera (21). Using our minimally invasive approach to the mouse retina through the sclera (*SI Appendix* Fig. S3 *A* and *B*), we found that the sheet structure of the nerve fiber layer allowed us to keep the plane of the nerve fiber layer parallel to the *x,y*-plane of intravital imaging and to perform intravital sequential time-lapse imaging of mitochondrial transport in a single axon without *z*-stacks (MIMIR, Movie S4). With submicrometer resolution, MIMIR showed that the axonal transport of mitochondria was highly dynamic over 5 min without losing focus in vivo (Fig. 1 *A* and *B* and Movie S4), a result clearly different from that seen in the retinal explants (Movie S1). Time-lapse imaging, which was acquired every 3 s without *z*-stacks, shows that MIMIR did not cause phototoxicity over 5 min (Movie S4). Immunohistochemistry for GFAP (*SI Appendix*, Fig. S4 *A*–*C*), a marker of glial inflammation, and Annexin V staining (*SI Appendix*, Fig. S4 *D*–*F*), an early marker of apoptosis, in the MIMIR-imaged area of the retina showed that MIMIR did not induce glial-based inflammatory responses in the retina or RGC apoptosis. A kymograph of the axon (red parallel lines in Fig. 1*A*) revealed active axonal transport of mitochondria, shown as diagonal lines (Fig. 1*B*). Note that the kymograph (Fig. 1*B*) includes the transport of a mitochondrion that was less than 1 μm in length. Furthermore, axonal transport of mitochondria is sensitive to changes in the neuronal milieu. Intravital imaging of axons in the cerebral cortex would require thinning or opening of the skull (22); importantly, MIMIR does not require thinning or opening of the sclera (*SI Appendix*, Fig. S1*A*, blue) (which may be considered the ocular equivalent of the skull) or involve changes in the intraocular humor (which may be considered the ocular equivalent of the cerebrospinal fluid). The minimal invasiveness, short time-lapse interval, and avoidance of phototoxicity of MIMIR confirm that the axonal transport of mitochondria is highly dynamic in the mammalian CNS in vivo under physiological conditions.

We also observed mitochondria transported from and to the RGC cell body (Fig. 1 *C* and *D* and Movie S5). Using MIMIR, we imaged the peripheral retina, where all RGC axons are relatively close to the RGC cell bodies. Of the axons we observed by MIMIR, 16.7% were ≤125 μm from the soma. We found that the distance of mitochondrial transport was shorter in the axons ≤125 μm from the soma (*SI Appendix*, Fig. S5) than in the axons that were >125 μm from the soma. Moreover, MIMIR shows that characteristically long (>10 μm), snake-like mitochondria are transported smoothly through the curve of the RGC axon (Fig. 1 *E* and *F* and Movie S6). Different excitation intensity did not change the mitochondrial dynamics (*SI Appendix*, Fig. S6), suggesting that CFP emission by MIMIR does not affect the mitochondrial dynamics.

Ocular Hypertension Induces Glaucomatous Changes in Mouse RGCs. To examine disturbances of axonal transport of mitochondria in neurodegenerative models, we chose a mouse model of glaucoma, laser-induced ocular hypertension (OHT) (8). Intraocular pressure in adult (4-mo-old) OHT group increased 1 and 2 d after laser treatment as compared with that in adult control group (*SI Appendix*, Fig. S7*A*). The number of intact axons in cross-sections of optic nerves did not decrease significantly 3 d after treatment but did decrease significantly 14 d after treatment (*SI Appendix*, Fig. S7 *B*–*E*). Likewise, the density of Brn-3$^+$ RGCs in retinal whole mounts did not decrease significantly 3 d after treatment but did decrease significantly 14 d after treatment (*SI Appendix*, Fig. S7 *F*–*I*).

Disturbances of Mitochondrial Transport in the Glaucoma Model 3 d After Treatment in Vivo. The minimal invasiveness of MIMIR is an important advantage in studies of neurodegenerative models and aging in the CNS, because axonal transport of mitochondria is

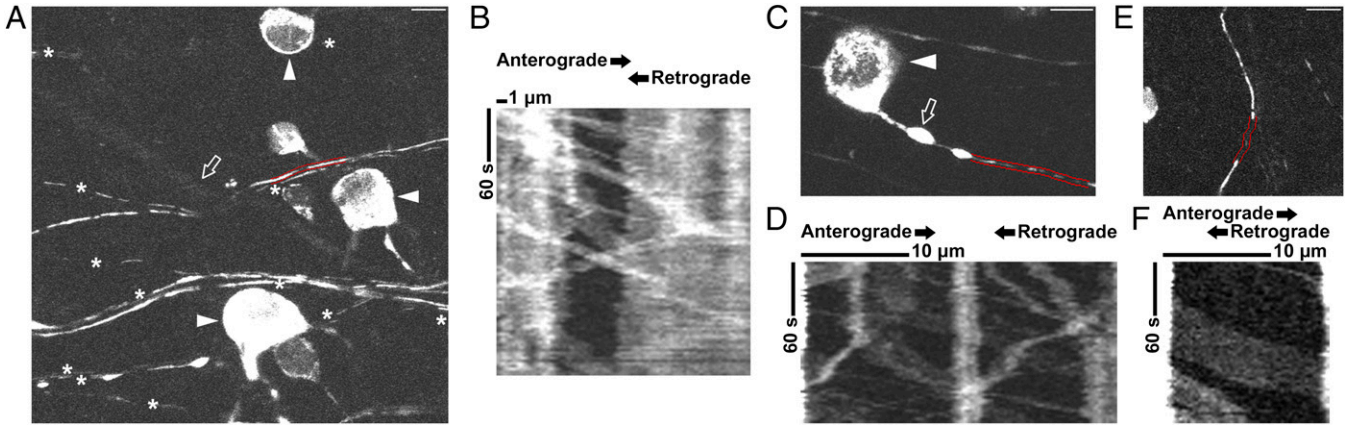

Fig. 1. The sheet structure of the nerve fiber layer permits intravital sequential time-lapse imaging of mitochondria transported in a single axon with submicrometer resolution, showing that axonal transport of mitochondria is highly dynamic in the mammalian CNS in vivo under physiological conditions and is clearly different from that seen in retinal explants. (*A*) Representative image obtained by MIMIR at submicrometer resolution, showing highly dynamic axonal transport of mitochondria with the focus maintained on axons, without artifacts caused by heartbeat and breathing, for 5 min under physiological conditions (Movie S4). The open arrow indicates a retinal vessel; arrowheads indicate RGC cell bodies; asterisks indicate RGC axons. (Scale bar, 10 μm.) (*B*) A kymograph of the axon indicated by red parallel lines in *A* detected active axonal transport of mitochondria shown as diagonal lines. Note that this kymograph includes transport of a mitochondrion that was less than 1 μm in length. (*C*) Representative image of MIMIR from Movie S5, showing that mitochondria are transported from and to the RGC cell body (arrowhead). Note that the first varicosity (open arrow) from the RGC cell body is plainly larger than the second varicosity. (Scale bar, 10 μm.) (*D*) A kymograph of the axon indicated by red parallel lines in *C* detects anterograde and retrograde axonal transport of mitochondria. (*E*) Representative image of MIMIR (Movie S6) showing that characteristically long, snake-like mitochondria are transported smoothly through the curve of the RGC axon. (Scale bar, 10 μm.) (*F*) A kymograph of the axon indicated by red parallel lines in *E* indicates that the length of the first snake-like mitochondrion is greater than 10 μm.

more sensitive to changes in the milieu of diseased and aged neurons. To investigate how the axonal transport of mitochondria is disturbed in mice with experimental glaucoma, we performed MIMIR of adult (4-mo-old) control mice (Fig. 2 *A* and *B* and Movie S7) and adult mice with experimental glaucoma 3 d after treatment (Fig. 2 *C* and *D* and Movie S8). In adult control mice we observed active axonal transport of mitochondria (Movie S7). However, MIMIR of the adult mice with experimental glaucoma 3 d after treatment showed an axon (asterisk) in which mitochondrial transport decreased and mitochondria-free regions increased, although an axon (double asterisk) with active transport and preserved blood flow (open arrow) were observed also (Movie S8). A kymograph of the axon (red parallel lines in Fig. 2*C*) confirmed reduced axonal transport of mitochondria (Fig. 2*D*). To characterize the disturbances of axonal transport of mitochondria in the glaucoma model, we compared the mitochondrial dynamics in control and OHT mice. We found that OHT decreased the number of mitochondria transported in axons (Fig. 2*E*) and both anterograde (Fig. 2*F*) and retrograde (Fig. 2*G*) transport. However, OHT did not disturb the duration of transport (Fig. 2*H*), distance of transport (Fig. 2*I*), duty cycle (the percentage of time spent in transport; Fig. 2*J*), or transport velocity (Fig. 2*K*). OHT increased the mitochondria-free regions in axons (Fig. 2*L*) and decreased the length of mitochondria transported in axons (Fig. 2*M*). As measured by real-time RT-PCR, mRNA expression of a key transcriptional coactivator [peroxisome proliferator-activated receptor γ coactivator-1α (PGC-1α)] and a transcription factor [nuclear respiratory factor 1 (NRF-1)] of mitochondrial biogenesis decreased 3 d after RGC axon injury (*SI Appendix*, Fig. S8 *A* and *B*) compared with their expression in control retinas. This finding suggests that RGC axon injury induces a decrease in mitochondrial biogenesis in RGCs. This decrease in mitochondrial biogenesis may result in the increased mitochondria-free regions observed in the RGC axons of OHT mice.

We detected the reduction in axonal transport of mitochondria in CFP-expressing RGCs in the early stage of the glaucoma model (3 d after laser treatment), when RGC death was not dominant. Histological studies in DBA/2J mice, a mouse model of pigmentary glaucoma (23), showed that retrograde axonal transport of Fluoro-Gold is impaired before RGC axon loss and RGC death (24) occur and that RGC axons persist well after anterograde axonal transport of cholera toxin B fails (25). Together with these findings, our results suggest that a decrease in intrinsic axonal transport of mitochondria occurs before RGC death in glaucoma.

Age-Related Changes in the Axonal Transport of Mitochondria in Vivo. The minimal invasiveness of our method enabled us to perform MIMIR in middle-aged (12- to 13-mo-old) (Fig. 3 *A* and *B* and Movie S9) and old (23- to 25-mo-old) mice (Fig. 3 *C* and *D* and Movie S10). In middle-aged and old mice (Movies S9 and S10), we observed active mitochondrial transport in axons (asterisks) with preserved blood flow (open arrows). Kymographs (red parallel lines in Fig. 3 *A* and *C*) reveal active axonal transport of mitochondria (Fig. 3 *B* and *D*). To characterize age-related changes in the axonal transport of mitochondria, we compared the mitochondrial dynamics in young (2-mo-old), adult (4-mo-old), middle-aged, and old mice. The number of mitochondria transported in axons of middle-aged and old mice did not change in the anterograde or retrograde directions (Fig. 3 *E*–*G*). However, in contrast with the glaucoma model in adult mice, the duration (Fig. 3*H*) and distance (Fig. 3*I*) of transport decreased with aging. Consistent with this decrease, the duty cycle also decreased with aging (Fig. 3*J*). The averages of transport velocity in each of the four age groups converged toward ∼0.2 μm/s (Fig. 3*K*). The mitochondria-free regions in axons increased with aging, compared with those in young mice (Fig. 3*L*). The length of mitochondria transported in axons decreased with aging (Fig. 3*M*).

To check the visual function of the albino line of *Thy1-mitoCFP-S* mice, we conducted electroretinograms in adult, middle-aged, and old mice (*SI Appendix*, Fig. S9). The results suggest that the firing rates of RGCs in old mice may decrease compared with those in adult mice. However, previous studies have shown that low firing rates in neurons accelerate mitochondrial movement (16, 26), because the mitochondria do not have to stop in metabolically inactive axons. These results

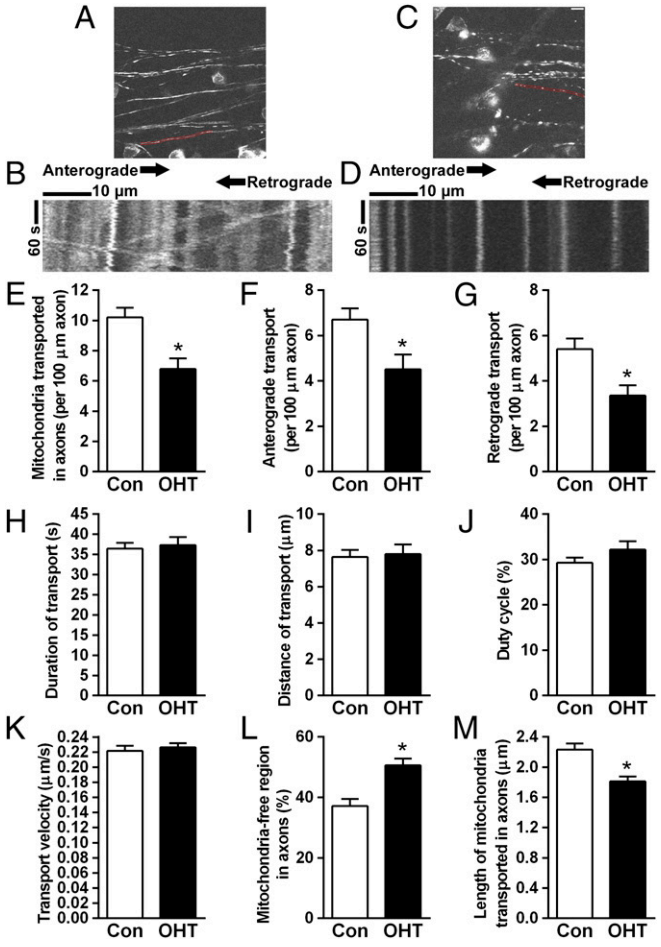

Fig. 2. MIMIR reveals disturbances of mitochondrial transport in the glaucoma model 3 d after treatment in vivo. (*A*) A representative image from Movie S7 showing MIMIR of an adult (4-mo-old) control mouse. (*B*) A kymograph of the axon indicated by red parallel lines in *A* detected active axonal transport of mitochondria shown as diagonal lines. (*C*) A representative image from Movie S8 showing MIMIR of an adult mouse with experimental glaucoma 3 d after laser treatment. (Scale bar, 10 μm.) (*D*) A kymograph of the axon indicated by red parallel lines in *C* shows that the number of transported mitochondria in the axon decreased and mitochondria-free regions increased. (*E*) OHT decreased the number of mitochondria transported in axons 3 d after laser treatment; $*P <$ 0.0001. (*F* and *G*) OHT decreased anterograde (*F*, $*P < 0.0001$) and retrograde (*G*, $*P = 0.001$) transport. (*H–K*) OHT did not disturb the duration of transport (*H*), distance of transport (*I*), duty cycle (i.e., the percentage of time spent in transport) (*J*), or transport velocity (*K*). (*L*) OHT increased the mitochondria-free regions in axons; $*P = 0.0001$. (*M*) OHT decreased the length of mitochondria (the length parallel to the axonal long axis) transported in axons. $*P = 0.007$. The two-tailed Mann–Whitney test was used to calculate *P* values in *E–M*. The results are shown as mean ± SEM. The sample size (*n*) for each group is given in *SI Appendix*, Table S1.

suggest that the age-related shortening of mitochondrial transport does not result from changes in RGC firing rates. Additionally, no significant dose-dependent effects of ketamine (120–180 mg/kg) on the dynamics of axonal transport of mitochondria were observed in adult or old mice (*SI Appendix*, Fig. S10), suggesting that the shorter mitochondrial transport in old mice relative to adult mice does not result from different depths of anesthesia in adult and old mice in MIMIR.

Enzyme activities of electron transfer complexes I and IV diminish selectively in brain mitochondria of middle-aged (12-mo-old) mice (27). In the brains of aged (24.5-mo-old) rats the enzyme activity of carnitine acetyltransferase, a key enzyme for transport of acetyl moieties to mitochondria for oxidation, decreases (28). These age-related reductions in the activity of enzymes necessary for

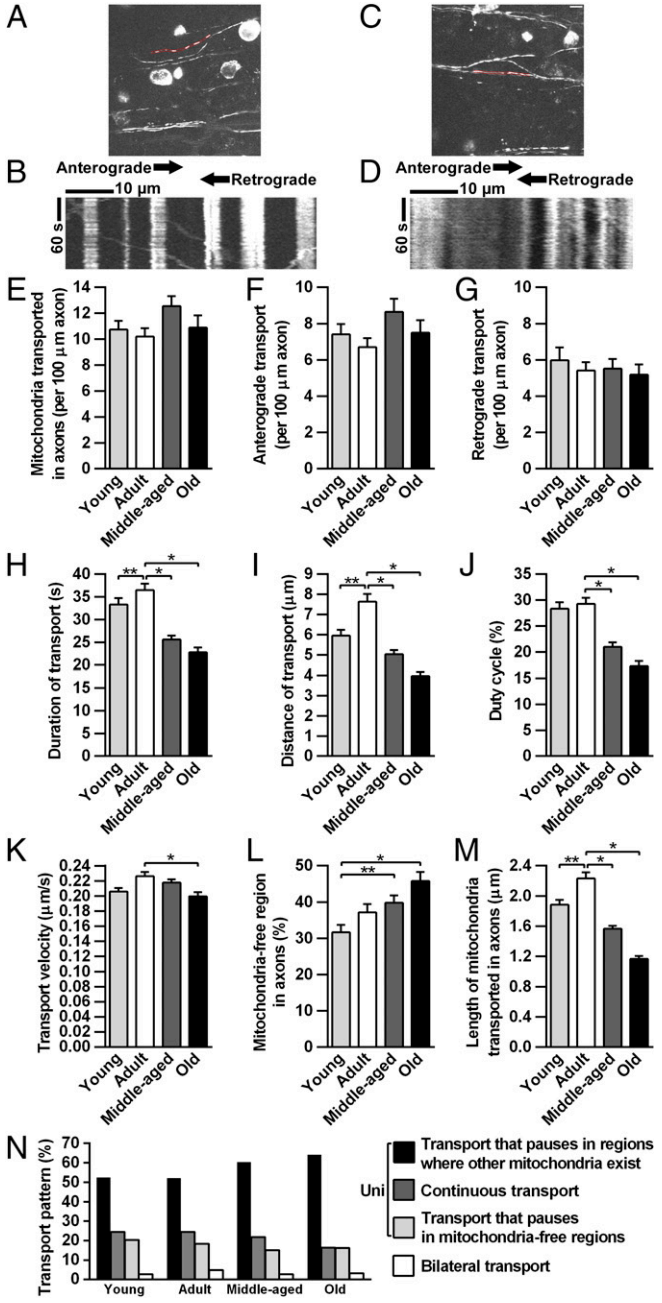

Fig. 3. MIMIR of middle-aged (12- to 13-mo-old) and old (23- to 25-mo-old) mice reveals age-related changes in axonal transport of mitochondria in vivo. (*A–D*) MIMIR of middle-aged (*A* and Movie S9) and old (*C* and Movie S10) mice. (Scale bar in *C*, 10 μm.) The kymographs detected active axonal transport of mitochondria in middle-aged (*B*) and old (*D*) mice. (*E–G*) The number of mitochondria transported in axons (*E*) and anterograde (*F*) and retrograde (*G*) transport did not change with age. (*H–J*) The duration (*H*, $*P < 0.0001$, $**P =$ 0.04) and distance (*I*, $*P < 0.0001$, $**P = 0.0005$) of transport and the duty cycle (*J*, $*P < 0.0001$) decreased with aging. (*K*) The averages of the transport velocity in the four age groups converged toward ∼0.2 μm/s; $*P = 0.02$. (*L*) The mitochondria-free regions in axons increased with aging; $*P = 0.0002$, $**P = 0.02$. (*M*) The length of mitochondria transported in axons decreased with aging; $*P < 0.0001$, $**P = 0.0006$. Dunn's two-tailed test was used in *E–M*. (*N*) Similar proportions of the four transport patterns through the four age groups suggest totally organized transport patterns are preserved in old mice. The sample size (*n*) is given in *SI Appendix*, Table S1.

energy production by mitochondria may lead to the overall short axonal transport of mitochondria in middle-aged and old mice.

To describe the dynamics of axonal transport of mitochondria in more detail, we defined four transport patterns (*SI Appendix*, Fig. S11 and Movies S11–S14): bilateral transport, continuous transport, transport that pauses in regions where other mitochondria exist, and transport that pauses in mitochondria-free regions. We observed similar proportions of the four transport patterns among the four age groups (Fig. 3*N*), indicating that almost all mitochondria were unidirectionally transported in vivo (young, 97.3%; adult, 95.1%; middle-aged, 97.2%; and old, 96.8%). Further, we found that the ratios of anterograde transport to retrograde transport were consistent (~3:2) among the four age groups (*SI Appendix*, Fig. S11*I*). In contrast to the age-related changes, these results indicate that the totally organized patterns of mitochondrial transport consistently observed in the RGCs of young, adult, and middle-aged mice are preserved in the RGCs of old mice and suggest that the machinery and basic function of axonal transport of mitochondria and homeostasis are preserved in normal aged neurons in the mammalian CNS in vivo.

Axonal Transport of Mitochondria in Old Mice Is Vulnerable to the Glaucoma Model. Finally, to study the susceptibility of axonal transport of mitochondria to the glaucoma model in old mice, we performed MIMIR of 23- to 25-mo-old OHT mice 3 d after treatment (Fig. 4*A* and Movie S15). The number of mitochondria transported in axons (Fig. 3*E*) and anterograde (Fig. 3*F*) and retrograde (Fig. 3*G*) transport did not change in old control mice relative to adult control mice. However, we observed significant decreases in the number of mitochondria transported in axons (Fig. 4*B*) and anterograde (Fig. 4*C*) and retrograde (Fig. 4*D*) transport in old OHT mice compared with those numbers in adult OHT mice. These results suggest that in old mice the axonal transport of mitochondria is more vulnerable to the glaucoma model than in adult mice. The reductions (Fig. 4 *B–D*) likely occurred before axon degeneration because they were detected in RGC axons, all of which retained CFP (Movie S15). In a *Thy1*-CFP DBA/2J mouse line, the loss of CFP is concurrent with RGC neurodegeneration (29). Further, the greater decreases (Fig. 4 *B–D*) in old OHT mice as compared with adult OHT mice may reflect accelerated axon damage in old mice, because RGC axons in old mice have a vulnerability to stresses resulting from the presence of more mitochondria-free regions (*SI Appendix*, Fig. S12) and decreased mitochondrial lengths (Fig. 3*M*) in axons relative to adult mice. The increase in mitochondria-free regions in axons indicates an increase in regions inadequately supported by mitochondria.

Discussion

In this study, we took advantage of the excellent accessibility of the albino mouse retina for intravital imaging and of the planar structure of the nerve fiber layer, which facilitates keeping the focal *x,y*-plane of the intravital imaging on the nerve fiber layer. We show that MIMIR enables sequential time-lapse imaging of mitochondria transported in a single axon with submicrometer resolution, maintaining focus on the axon in vivo. MIMIR not only confirms that axonal transport of mitochondria is highly dynamic in the mammalian CNS in vivo under physiological conditions but also allows characterization of the dynamics of axonal transport of mitochondria in the diseased and aged mammalian CNS in vivo, revealing a specific vulnerability of mitochondrial transport to the glaucoma model in aged mice.

For the study of axonal transport of mitochondria, it is worth noting that intravital imaging offers benefits over explant imaging because (*i*) axonal transport of mitochondria is quite sensitive to changes in the milieu of neurons; (*ii*) intravital imaging allows true in vivo observations; (*iii*) intravital imaging can be performed under physiological oxygen levels and metabolism; and (*iv*) intravital imaging can be performed with intact blood flow and neural innervation (30). Indeed, the mitochondrial dynamics shown by explant imaging of the retina (rare axonal transport of mitochondria and excessive mitochondrial fragmentation; Movie S1) are clearly different from those shown by MIMIR in vivo, even though the retinal explants were obtained and maintained under conditions optimized for long-term retinal cultures, as described previously (31). MIMIR does not involve thinning or opening of the sclera or changes in the intraocular humor. Moreover, the 2D structure of the nerve fiber layer parallel to the *x,y* plane of intravital imaging enables us to maintain focus on RGC axons and obtain sequential time-lapse images of mitochondria transported in a single axon without *z*-stacks. The absence of *z*-stacks permits a short and regular time-lapse interval (3 s), which has been shown to yield reliable data on the dynamics of axonal transport of mitochondria (32).

Aging is a major risk factor for the incidence of neurodegenerative diseases of the CNS (3, 4), including glaucoma (5). Our findings of overall short transport, increased mitochondria-free regions, and decreased mitochondrial length in middle-aged and old mice (Fig. 3 *H–J*, *L*, and *M* and *SI Appendix*, Fig. S12) suggest that the capacity to resist stresses (33) decreases in RGCs with aging (blue solid line in Fig. 4*E*). Our findings regarding the vulnerability of axonal transport of mitochondria to the glaucoma model in old mice compared with that in adult mice (Fig. 4 *B–D*) may result from a lower threshold that leads to metabolic dysfunction of RGCs in old mice (orange dotted line and asterisk

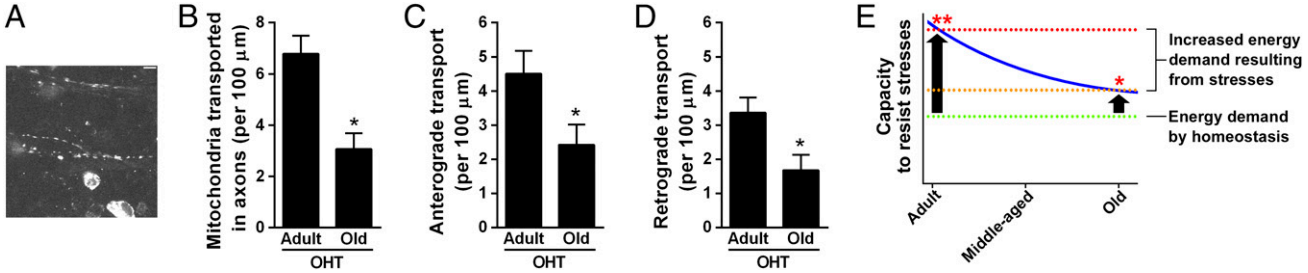

Fig. 4. MIMIR shows that axonal transport of mitochondria is more vulnerable to the glaucoma model in old mice than in adult mice. (*A*) A representative image showing MIMIR in an old OHT mouse (Movie S15). (Scale bar, 10 µm.) (*B–D*) In old OHT mice, we observed significant decreases in the number of mitochondria transported in axons (*B*) and in anterograde (*C*) and retrograde (*D*) transport as compared with adult OHT mice; $*P < 0.0001$. (*E*) The capacity to resist stresses in RGCs (solid blue line) is estimated by age-related changes in the duty cycle in Fig. 3*J*. Our results regarding the total organization of mitochondrial transport (Fig. 3*N* and *SI Appendix*, Fig. S11) suggest that the energy demand by homeostasis (green dotted line) does not exceed the capacity to resist stresses even in the RGCs of old mice. However, our results regarding the vulnerability of the axonal transport of mitochondria to the glaucoma model in old mice (*B–D*) suggest that the lower increase in energy demand resulting from stresses such as elevated intraocular pressure (orange dotted line) leads to metabolic dysfunction of RGCs in old mice (asterisk) as compared with adult mice (red dotted line and double asterisk). The two-tailed Mann–Whitney test was used to calculate *P* values in *B–D*. The results are shown as mean ± SEM. The sample size (*n*) for each group is given in *SI Appendix*, Table S1.

in Fig. 4*E*) compared with that in adult mice (red dotted line and double asterisk in Fig. 4*E*). Therefore, a reduction in the capacity to resist stresses with aging, caused by decreased energy production and support by mitochondria, may contribute to the age-related increase in glaucoma incidence.

Tissue transparency (minimal absorption and scattering of light), available mainly in zebrafish in vivo or by using chemical reagents to clear fixed samples (34), has facilitated imaging studies of the CNS. MIMIR is unique in intravital imaging of the mammalian CNS. First, we used C57BL/6 background *Thy1-mitoCFP* mice for intravital imaging of RGCs but could not acquire RGC images through the sclera because of uveal pigmentation. Therefore, we backcrossed each line of *Thy1-mitoCFP* mice with BALB/c mice. However, we should consider that the dynamics of axonal transport of mitochondria may differ among mouse strains. To generalize our current findings regarding age-related shortening of mitochondrial transport to other mouse strains that are more commonly used in vision research, such as C57BL/6 mice, it will be necessary to develop intravital imaging of the retina at submicrometer resolution in these strains; however, an age-related decrease in the electroretinogram amplitude also has been observed in C57BL/6 mice (35). We used the retina, a sensory organ, because the planar structure of the retina is necessary for MIMIR. However, the mouse retina is sensitive to light at levels approaching a single photon, as is the human retina (36). We should take into account that intravital imaging of the retina using fluorescence could induce neural activity and that the firing rates of neurons are related to mitochondrial dynamics (16). Moreover, because the human uvea cannot be made transparent, the current MIMIR method is not applicable to humans. Rather, in humans the retina must be imaged via the cornea, and the long working distance necessary for intravital imaging of the retina through the cornea makes the use of objectives with high numerical aperture difficult. Using an objective (0.5 numerical aperture) with adaptive optic systems and an original algorithm, intravital imaging through the cornea shows fluorescent granules in the mouse retinal pigment epithelium (37). However, we believe that our approach of intravital sequential time-lapse imaging of submicrometer structures in RGC axons through the sclera allows us to detect early glaucomatous changes and understand the mechanisms of glaucoma pathology and aging. The understanding gained by our approach through the sclera may lead to the prediction of RGC death in glaucoma patients by intravital imaging of the retina through the cornea. Thus, MIMIR provides previously unrecognized insights not only into the fundamental dynamics of axonal transport of mitochondria but also into neurodegeneration and aging in the mammalian CNS in vivo.

Materials and Methods

We performed all experiments according to the protocols approved by the Kumamoto University and University of Fukui Institutional Animal Care Committees and in accordance with the Association for Research in Vision and Ophthalmology's Statement for the Use of Animals in Ophthalmic and Vision Research. Methods for all experiments are described in detail in *SI Appendix*.

ACKNOWLEDGMENTS. We thank F. Suzuki, H. Takagi, Y. Kusaka, H. Takebayashi, W-J Song, H. Hayashi, M. Inoue, M. Iwao, Y. Takatsuru, T. Fujimoto, S. Yokota, T. Tomomatsu, T. Matsumura, S. Arimura, and M. Gozawa for advice on experiments and Y. Nakaishi-Fukuchi, C. Naito, M. Miyagawa, A. Koshide, and T. Yamamoto for excellent technical assistance. This work was supported by grants from the Ministry of Education, Culture, Sports, Science and Technology (MEXT) of Japan (to M.I., H.T., and Y. Takihara), grants from the Ministry of Health, Labor and Welfare of Japan (to M.I.), research grants from the University of Fukui (to Y. Takihara), and the Global Centers of Excellence Program (Cell Fate Regulation Research and Education Unit), MEXT of Japan (to H.T.).

1. Resnikoff S, et al. (2004) Global data on visual impairment in the year 2002. *Bull World Health Organ* 82(11):844–851.
2. Quigley HA, Broman AT (2006) The number of people with glaucoma worldwide in 2010 and 2020. *Br J Ophthalmol* 90(3):262–267.
3. Hebert LE, et al. (1995) Age-specific incidence of Alzheimer's disease in a community population. *JAMA* 273(17):1354–1359.
4. Van Den Eeden SK, et al. (2003) Incidence of Parkinson's disease: Variation by age, gender, and race/ethnicity. *Am J Epidemiol* 157(11):1015–1022.
5. Leske MC, Wu SY, Hennis A, Honkanen R, Nemesure B; BESs Study Group (2008) Risk factors for incident open-angle glaucoma: The Barbados Eye Studies. *Ophthalmology* 115(1):85–93.
6. Vrabec JP, Levin LA (2007) The neurobiology of cell death in glaucoma. *Eye (Lond)* 21(Suppl 1):S11–S14.
7. Radius RL, Anderson DR (1981) Rapid axonal transport in primate optic nerve. Distribution of pressure-induced interruption. *Arch Ophthalmol* 99(4):650–654.
8. Fu CT, Sretavan DW (2012) Ectopic vesicular glutamate release at the optic nerve head and axon loss in mouse experimental glaucoma. *J Neurosci* 32(45):15859–15876.
9. Hirokawa N, Takemura R (2005) Molecular motors and mechanisms of directional transport in neurons. *Nat Rev Neurosci* 6(3):201–214.
10. Saxton WM, Hollenbeck PJ (2012) The axonal transport of mitochondria. *J Cell Sci* 125(Pt 9):2095–2104.
11. Stokin GB, et al. (2005) Axonopathy and transport deficits early in the pathogenesis of Alzheimer's disease. *Science* 307(5713):1282–1288.
12. Chan DC (2006) Mitochondria: Dynamic organelles in disease, aging, and development. *Cell* 125(7):1241–1252.
13. Vossel KA, et al. (2010) Tau reduction prevents Abeta-induced defects in axonal transport. *Science* 330(6001):198.
14. Green DR, Galluzzi L, Kroemer G (2011) Mitochondria and the autophagy-inflammation-cell death axis in organismal aging. *Science* 333(6046):1109–1112.
15. Pilling AD, Horiuchi D, Lively CM, Saxton WM (2006) Kinesin-1 and Dynein are the primary motors for fast transport of mitochondria in *Drosophila* motor axons. *Mol Biol Cell* 17(4):2057–2068.
16. Ohno N, et al. (2011) Myelination and axonal electrical activity modulate the distribution and motility of mitochondria at CNS nodes of Ranvier. *J Neurosci* 31(20):7249–7258.
17. Misgeld T, Kerschensteiner M, Bareyre FM, Burgess RW, Lichtman JW (2007) Imaging axonal transport of mitochondria in vivo. *Nat Methods* 4(7):559–561.
18. Plucińska G, et al. (2012) In vivo imaging of disease-related mitochondrial dynamics in a vertebrate model system. *J Neurosci* 32(46):16203–16212.
19. Yin L, et al. (2013) Imaging light responses of retinal ganglion cells in the living mouse eye. *J Neurophysiol* 109(9):2415–2421.
20. Shepherd GM, Harris KM (1998) Three-dimensional structure and composition of CA3–>CA1 axons in rat hippocampal slices: Implications for presynaptic connectivity and compartmentalization. *J Neurosci* 18(20):8300–8310.
21. Imanishi Y, Batten ML, Piston DW, Baehr W, Palczewski K (2004) Noninvasive two-photon imaging reveals retinyl ester storage structures in the eye. *J Cell Biol* 164(3):373–383.
22. Xu HT, Pan F, Yang G, Gan WB (2007) Choice of cranial window type for in vivo imaging affects dendritic spine turnover in the cortex. *Nat Neurosci* 10(5):549–551.
23. Chang B, et al. (1999) Interacting loci cause severe iris atrophy and glaucoma in DBA/2J mice. *Nat Genet* 21(4):405–409.
24. Buckingham BP, et al. (2008) Progressive ganglion cell degeneration precedes neuronal loss in a mouse model of glaucoma. *J Neurosci* 28(11):2735–2744.
25. Crish SD, Sappington RM, Inman DM, Horner PJ, Calkins DJ (2010) Distal axonopathy with structural persistence in glaucomatous neurodegeneration. *Proc Natl Acad Sci USA* 107(11):5196–5201.
26. Li Z, Okamoto K, Hayashi Y, Sheng M (2004) The importance of dendritic mitochondria in the morphogenesis and plasticity of spines and synapses. *Cell* 119(6):873–887.
27. Navarro A, Boveris A (2007) The mitochondrial energy transduction system and the aging process. *Am J Physiol Cell Physiol* 292(2):C670–C686.
28. Liu J, Killilea DW, Ames BN (2002) Age-associated mitochondrial oxidative decay: Improvement of carnitine acetyltransferase substrate-binding affinity and activity in brain by feeding old rats acetyl-L- carnitine and/or R-alpha -lipoic acid. *Proc Natl Acad Sci USA* 99(4):1876–1881.
29. Raymond ID, Pool AL, Vila A, Brecha NC (2009) A Thy1-CFP DBA/2J mouse line with cyan fluorescent protein expression in retinal ganglion cells. *Vis Neurosci* 26(5-6):453–465.
30. Germain RN, Miller MJ, Dustin ML, Nussenzweig MC (2006) Dynamic imaging of the immune system: Progress, pitfalls and promise. *Nat Rev Immunol* 6(7):497–507.
31. Johnson TV, Martin KR (2008) Development and characterization of an adult retinal explant organotypic tissue culture system as an in vitro intraocular stem cell transplantation model. *Invest Ophthalmol Vis Sci* 49(8):3503–3512.
32. De Vos KJ, et al. (2007) Familial amyotrophic lateral sclerosis-linked SOD1 mutants perturb fast axonal transport to reduce axonal mitochondria content. *Hum Mol Genet* 16(22):2720–2728.
33. Toescu EC (2005) Normal brain ageing: Models and mechanisms. *Philos Trans R Soc Lond B Biol Sci* 360(1464):2347–2354.
34. Hama H, et al. (2011) Scale: A chemical approach for fluorescence imaging and reconstruction of transparent mouse brain. *Nat Neurosci* 14(11):1481–1488.
35. Li C, Cheng M, Yang H, Peachey NS, Naash MI (2001) Age-related changes in the mouse outer retina. *Optom Vis Sci* 78(6):425–430.
36. Naarendorp F, et al. (2010) Dark light, rod saturation, and the absolute and incremental sensitivity of mouse cone vision. *J Neurosci* 30(37):12495–12507.
37. Palczewska G, et al. (2014) Noninvasive two-photon microscopy imaging of mouse retina and retinal pigment epithelium through the pupil of the eye. *Nat Med* 20(7):785–789.